Numerical prediction of laminar flow and heat transfer characteristics in a tube fitted with regularly spaced twisted-tape elements

A. W. Date and S. K. Saha
Mechanical Engineering Department, Indian Institute of Technology, Bombay, India

By numerically solving the Navier–Stokes and energy equations in their three-dimensional parabolic form, the friction and heat transfer characteristics are predicted for laminar flow in a circular tube fitted with regularly spaced twisted-tape elements that are connected by circular rods. The predictions have agreed closely with the experimental data for water. It is shown that a strong L/D effect is associated with the configuration under consideration. By extending the predictions outside the range of experimental data, it is found that considerably enhanced thermohydraulic performance is achievable by increasing the number of turns on the tape elements, by reducing the connecting rod diameter, and at high fluid Prandtl numbers.

Keywords: laminar flow; circular tube; twisted-tape elements; forced convection

1. Introduction

The problem

Characteristics of fully developed and developing laminar flow in a tube containing a full-length, twisted-tape were predicted by Date.[1,2] Subsequently, experimental work carried out with axially uniform wall heat flux conditions by Hong and Bergles[3] and Sukhatme *et al.*[4] confirmed the validity of Date's fully developed flow predictions† for friction factor and Nusselt number, the latter for Pr'10.

This article deals with a new variant of the well-established, full-length, twisted-tape configuration. The new configuration consists of a circular tube fitted with regularly spaced twisted-tape elements that are connected by thin circular rods. The tape elements may have any number of turns (say, m). Figure 1, shows the configuration for $m=1$. Each tape section extends over a distance mH, where H is the axial length for 180° rotation of the tape. The two successive tape elements are joined by a thin rod of diameter d and length S. The rod section is thus annular in cross section. For purposes of discussion, each combination of tape and annular sections is termed a module.

Characteristics of laminar flow and heat transfer in this new configuration have been experimentally investigated by Saha *et al.*[6] and semiempirically analyzed by Date and Gaitonde.[7] These characteristics, however, have not been predicted by direct solution of the fundamental Navier–Stokes and energy equations. Such an effort has appeared worthwhile, as experimental investigations showed several unique features.

Saha *et al.*'s[6] pressure-drop measurements were made in a 13-mm i.d. perspex tube 1,800 mm long ($L/D \simeq 142$). The experiments were performed for $m=1$, for which the number of modules was $142/(y+s)$, where $y=H/D$ and $s=S/D$. The values of y chosen were 10, 7.5, 5.0, and 3.46. For each y, four values of s (10, 7.5, 5.0, and 2.5) were chosen. The thickness of the stainless steel tape elements was 0.4 mm (or $\delta/D=0.03077$), and the connecting-rod diameter d was 3 mm (or $d/D=0.2307$).

Heat transfer measurements were made in an 11-mm i.d. stainless steel tube with $\delta/D=0.03636$ and $d/D=0.2727$. The tube was electrically heated with nichrome wire, and the tape elements were covered at their edges with a steel-grid tape to prevent uncertainties caused by fin action. The heated section was 1,840 mm long (or $L_{\text{heated}}/D=167.3$). The test section provided axially uniform heat flux conditions with negligible circumferential variation in wall temperature at any cross section.

All measurements were carried out with water ($\text{Pr} \simeq 5$) as the working fluid. The uncertainties associated with the measurement of Nusselt number were estimated at 9 percent, whereas those for the friction factor were estimated at 6 percent.

Pressure-drop measurements showed that, although the pressure drops over the tape and the annulus sections were different, the module pressure drops reached a constant value—typically after 3 to 4 modules from the inlet section. The constancy of the pressure drop over a module represents the state of "periodically fully developed" flow. This state, however, does not imply vanishing axial derivatives of the velocities, because the flow in each section continues to be in a state of "development." It does imply that the velocity distributions at cross sections separated by distance $(mH+S)$ are identical when the periodically fully developed state is attained. Similarly, the length-averaged Nusselt numbers over a module can be expected to reach a constant value, indicating a "thermally periodically fully developed" condition. In the present experiment, wall temperatures were measured at only 16 well-spaced locations, with each thermocouple representing at least one module. The overall length-averaged Nusselt numbers evaluated in this way did indeed demonstrate near constancy with axial length.

Further, if the wall shear effects in the twisted-tape and the annular sections were the same, then it would normally be expected that the pressure drop associated with the present geometry will be lower than that obtained with full-length tapes when the surface area of the connecting rod (πdS) is smaller than that of the twisted tape ($2mDH$). Saha *et al.*,[6] however, found lowering of the pressure drop only for large spacings ($s=10$) for all twist ratios (y). For $s<10$, the pressure drops in fact were higher than those that would have been encountered for full-length, twisted tapes. Date and Gaitonde[7] explained that this increase is caused by the additional momentum-change losses associated with the developing character of the flow in the annular and twisted-tape sections, even when the flow was

† Date's[1] predictions of Nusselt number had to be augmented by a factor of 2, as pointed out in,[5] as there was a computational error in the final evaluation of the Nusselt number.

Address reprint requests to Dr. Date at the Mechanical Engineering Department, Indian Institute of Technology, Bombay, India.

Received 18 July 1989; accepted 17 May 1990

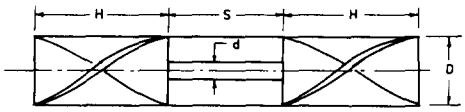

Figure 1 Geometry under investigation

periodically fully developed. Similarly, the measured Nusselt numbers were found to be either equal or lower than those for full-length tape for $s=10$. For closer spacings, however, the Nusselt numbers were greater than those for full-length tapes. For the same Reynolds number, the increase in heat transfer was typically greater than the increase in pressure drop. Thus the new configuration appears to be superior to the full-length tape for water ($\mathrm{Pr}\simeq 5.0$). For example, at $y=5$ and $s=2.5$, the new configuration showed a 47 percent increase in heat transfer for the same pumping power and a nearly 70 percent reduction in pumping power for the same heat duty at $\mathrm{Pr}=5.0$.[6]

Purposes and scope

One purpose of this article is to examine the experimental trends through numerical solution of the Navier–Stokes and the energy equations for the case of laminar flow in a tube containing regularly spaced twisted-tape elements connected by thin rods. As the experimental data of Saha *et al.*[6] were restricted to the case of $m=1$, $d/D\simeq 0.25$, and $\mathrm{Pr}\simeq 5.0$, a second purpose is to extend the predictions to different values of these parameters in order to indicate future directions for research.

The relevant mathematical formulation is described in section 2, where the governing equations are presented appropriate to the experiment. Section 3 presents comparisons of the predictions with the experimental data as well as some additional data to appreciate the local variations. This section further presents predictions that are extended to parametric values outside the range of the experimental data. Finally, the conclusions are reported in section 4.

2. Mathematical formulation

Governing equations

The twisted-tape section provides a geometry with two identical semicircular cross sections. The flow is diagonally symmetrical about the twisted tape. This diagonal symmetry continues even in the annular section, as such the flow in this section is periodic, with a period π. Hence the governing equations need to be solved only in a semicircular domain in both the tape and the annular sections. Figure 2 shows the typical configuration of a twisted-tape, annular-section module. For clarity, the tape is shown untwisted.

Because the flow remains in a state of development both in the inlet region and in the periodically fully developed region—and as the domain is semicircular—the flow can be described by three-dimensional (3-D) equations. At the inlet to each tape section, where the flow enters from the preceding annular section, a small region of axial circulation can be expected, because the flow has to "jump" from the connecting rod. Then, if the twist of the tape is high (small values of y), the downstream pressure distribution can be expected to influence the flow in the upstream direction. The first possibility renders the flow equations fully elliptic; the second, allows fully elliptic pressure alone to suffice. In the present paper, the possibility of axial circulation can be ignored if the rod diameter is assumed to be small. In any case, the region of axial circulation is also small enough to influence overall prediction of the pressure drop, which is of prime interest. Computations of Date[1] showed that for $y>3.14$, the full ellipticity of pressure need not be considered. In the present paper, computations are performed for $y>3.3$.

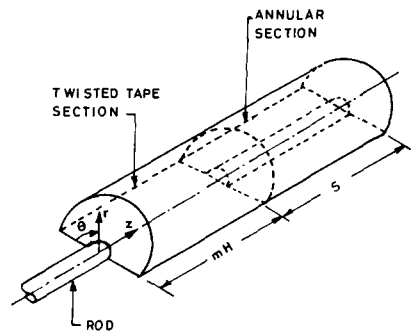

Figure 2 Tape–annular section module

Notation

d Connecting rod diameter
D Tube diameter
f Friction factor
r_r^* Dimensionless radial velocity, $2rV_r/D\bar{u}$
g_θ^* Dimensionless tangential velocity, $2rV_\theta/D\bar{u}$
H Twisted tape length for 180° rotation
h Heat transfer coefficient
k Thermal conductivity of the fluid
L Length of the test section
m Number of turns on the twisted tape
$\dot{m}$ Mass flow rate
Nu Nusselt number
p Pressure
p^* Dimensionless pressure, $p/\rho\bar{u}^2$
Pr Prandtl number, ν/α
Q_w Heat transfer rate per unit length
r Radial coordinate
r^* Dimensionless radius
Re Reynolds number, $\bar{u}D/\nu$
S Length of the annular section
s Space ratio, S/D
T Temperature
T^* $(T-T_{bi})/(Q_w/k)$
u Axial velocity
$\bar{u}$ Mean axial velocity
u^* Dimensionless axial velocity, $u/\bar{u}$
V_r Radial velocity
V_θ Tangential velocity
y Twist ratio, H/D
z Axial coordinate
z^* Dimensionless axial distance, $2z/D$

Greek symbols
α Thermal diffusivity
δ Thickness of the tape
θ Angular coordinate measured from the tape surface
ν Kinematic viscosity
ω Vorticity
ω^* Dimensionless vorticity, $\omega D/2\bar{u}$

Subscripts
b Bulk value
i Inner wall, inlet
w Wall
g Guessed value

Table 1 Coefficients in Equation (1) in the twisted-tape section

ϕ	a	b_1	b_2	S_ϕ
g_r^*	0	r^*	$\frac{1}{r^{*2}}$	$-\frac{\partial\omega^*}{\partial\theta}$ $+\frac{1}{r^*}\frac{\partial}{\partial r^*}\left[r^{*2}\left(\frac{\partial u^*}{\partial z^*}+\frac{\pi}{2y}\frac{\partial u^*}{\partial\theta}\right)\right]$
g_θ^*	0	r^*	$\frac{1}{r^{*2}}$	$\frac{1}{r^*}\frac{\partial(\omega^* r^{*2})}{\partial r^*}$ $+\frac{\partial}{\partial\theta}\left(\frac{\partial u^*}{\partial z^*}+\frac{\pi}{2y}\frac{\partial u^*}{\partial\theta}\right)$
u^*	1	$\frac{2r^*}{\mathrm{Re}}$	$\frac{2}{\mathrm{Re}}\left(\frac{1}{r^{*2}}+\frac{\pi^2}{4y^2}\right)$	S_{u^*}
ω^*	1	$\frac{2r^*}{\mathrm{Re}}$	$\frac{2}{\mathrm{Re}}\left(\frac{1}{r^{*2}}+\frac{\pi^2}{4y^2}\right)$	S_{ω^*}
T^*	1	$\frac{2r^*}{\mathrm{RePr}}$	$\frac{2}{\mathrm{RePr}}\left(\frac{1}{r^{*2}}+\frac{\pi^2}{4y^2}\right)$	$\frac{2\pi}{y\mathrm{PrRe}}\frac{\partial^2 T^*}{\partial\theta\,\partial z^*}$ $-\frac{\pi}{2y}\frac{\partial(u^*T^*)}{\partial\theta}$

where

$$S_{u^*}=-\frac{\partial\bar{p}^*}{\partial z^*}-\frac{\pi}{2y}\frac{\partial p_0^*}{\partial\theta}+\frac{2\pi}{\mathrm{Rey}}\frac{\partial^2 u^*}{\partial\theta\,\partial z^*}-\frac{\pi}{2y}\frac{\partial u^{*2}}{\partial\theta}$$

and

$$S_{\omega^*}=\frac{2\pi}{\mathrm{Rey}}\frac{\partial^2\omega^*}{\partial\theta\,\partial z^*}-\left(\frac{1}{r^{*2}}\frac{\partial u^*}{\partial\theta}\frac{\partial g_r^*}{\partial z^*}-\frac{1}{r^*}\frac{\partial u^*}{\partial r^*}\frac{\partial g_\theta^*}{\partial z^*}-\omega^*\frac{\partial u^*}{\partial z^*}\right)$$
$$-\frac{\pi}{2y}\left(\frac{1}{r^{*2}}\frac{\partial u^*}{\partial\theta}\frac{\partial g_r^*}{\partial\theta}-\frac{1}{r^*}\frac{\partial u^*}{\partial r^*}\frac{\partial g_\theta^*}{\partial\theta}+u^*\frac{\partial\omega^*}{\partial\theta}\right)$$

As such, the flow is assumed to be governed by 3-D parabolic assumptions. Further, the fluid properties are assumed to be uniform.

Date[2] transformed the 3-D parabolic Navier–Stokes and energy equations into a velocity-axial vorticity formulation, using a rotating coordinate system.[1] The equations can be described generally as follows:

$$\underbrace{a\left[\frac{1}{r^*}\frac{\partial}{\partial r^*}(g_r^*\phi)+\frac{1}{r^{*2}}\frac{\partial}{\partial\theta}(g_\theta^*\phi)+\frac{\partial}{\partial z^*}(u^*\phi)\right]}_{\text{(Convection)}}$$
$$=\underbrace{\left[\frac{1}{r^*}\frac{\partial}{\partial r^*}\left(b_1\frac{\partial\phi}{\partial r^*}\right)+\frac{\partial}{\partial\theta}\left(b_2\frac{\partial\phi}{\partial\theta}\right)\right]}_{\text{(Diffusion)}\quad\text{(Source)}}+\quad D_\phi \tag{1}$$

where a, b_1, b_2, and D for each variable ϕ are given in Table 1.

In Equation 1, consistent with the parabolic assumptions, the axial diffusion terms are neglected and the pressure p^* is represented as

$$p^*(r^*,\theta,z^*)=\bar{p}^*(z^*)+p_0^*(r^*,\theta)$$

The $\partial p_0^*/\partial\theta$ term in S_u^* is recovered from the tangential momentum equation, and the mean pressure $\bar{p}^*$ is recovered from satisfaction of mass flow rate conservation at each cross section. Note also that in a rotating coordinate system, the angle θ is always measured (clockwise in the present case) from the surface of the twisted tape and that the radial (r^*) and axial (z^*) coordinates retain their meaning in the fixed-frame system.

The coefficients given in Table 1 apply only to the twisted-tape section. In the annular section, all terms containing y must be dropped.

Boundary and initial conditions

The boundary conditions for the twisted-tape section ($0<z^*<$ my) are

$$g_r^*=g_\theta^*=u^*=0 \qquad \text{at } r^*=0,\ 1.0 \text{ and } \theta=0 \text{ and } \pi$$
$$\omega^*=-\frac{1}{r^*}\frac{\partial g_\theta^*}{\partial r^*} \qquad \text{at } r^*=0,\ 1.0 \tag{2}$$
$$\omega^*=\frac{1}{r^{*2}}\frac{\partial g_r^*}{\partial\theta} \qquad \text{at } \theta=0,\ \pi$$

The experiments of Saha *et al.*[6] were performed under axially uniform heat flux and nearly circumferentially uniform temperature conditions—and with insulated twisted tape—the temperature boundary conditions are

$$T^*=T_w^* \qquad \text{at } r^*=1.0$$
$$\frac{\partial T^*}{\partial r^*}=0 \qquad \text{at } r^*=0 \tag{3}$$
$$\frac{\partial T^*}{\partial\theta}=0 \qquad \text{at } \theta=0,\ \pi$$

The boundary conditions for the annular section ($0<z^*<s$)

are

$$g_r^* = g_\theta^* = u^* = 0 \qquad \text{at } r^* = r_i^* \text{ and } 1.0$$

$$\omega^* = -\frac{1}{r^*}\frac{\partial g_\theta}{\partial r^*} \qquad \text{at } r^* = r_i^* \text{ and } 1.0$$

The rod was connected to the tape elements, which were prevented from finning, and the rod was assumed to be thin. Thus zero flux was assumed at the surface of the rod under steady-state conditions, giving

$$T^* = T_w^* \qquad \text{at } r^* = 1.0$$

$$\frac{\partial T^*}{\partial r^*} = 0 \qquad \text{at } r^* = r_i^* \tag{4}$$

Further, because the flow and heat transfer are periodic in the annular section, for all ϕ

$$\phi|^{\theta=0} = \phi|_{\theta=\pi} \tag{5}$$

The governing equations for the flow variables were solved from the inlet section of the tube. The initial conditions at $z^* = 0$ were

$$u^* = 1.0$$
$$g_r^* = g_\theta^* = \omega^* = 0 \tag{6}$$

It will be easy to recognize that if the interest was confined only to the periodically fully developed region, then one could also solve Equation (1) with axially periodic conditions given by:

$$\phi|_{z'^*=0} = \phi|_{z'^*=2(my+s)} \tag{7}$$

This was, however, not done, as it was of interest to discover the number of modules (which were typically found to be 3 or 4 in the experiment of Saha *et al.*[6]) required for the attainment of the periodically fully developed state.

In the heat transfer predictions, the condition used at $z^* = 0$ was

$$T^* = T_w^* = 0 \tag{8}$$

This condition, of course, was not realized in the experiment, because some amount of axial conduction in the tube wall prevented equality of $T^* = T_w^*$ at the inlet. The condition was nonetheless used for reasons explained in the next section.

Prediction procedure

The governing equations, along with the boundary and initial conditions, were solved by a finite-difference technique in which the convective terms were represented in an upwind-difference form. The details of this technique are described in References 8 and 9.

Flow prediction

The calculations were begun in the twisted-tape section with a specified inlet pressure. The pressure at the downstream section (ΔZ^* away) was guessed ($\bar{P}_{d,g}^*$, say) and the equations for the flow variables were solved. Now the axial mass flow rate ($\dot{m}_g$) was estimated by integrating the u_g^* profile over the cross-section. The correction $\Delta\bar{P}^*$ to the guessed pressure $\bar{P}_{d,g}^*$ was assumed to be proportional to $(\dot{m}_{true} - \dot{m}_g)$. The estimated correction was applied to $\bar{P}_{d,g}^*$ in successive iterations until $\Delta\bar{P}^*$ was found to fall below 10^{-6}. Thus

$$R_m = \frac{1}{r^*}\frac{\partial g_r^*}{\partial r^*} + \frac{1}{r^{*2}}\frac{\partial g_\theta}{\partial \theta} + \frac{\partial u^*}{\partial z^*} + \frac{\pi}{2y}\frac{\partial u^*}{\partial \theta} \tag{9}$$

Typically, $\sum_{\text{all cells}} |R_m|$ was less than 10^{-4}. Moreover, the maximum absolute fractional change for each variable was less than 5×10^{-3}.

Between 15 and 50 iterations were required to achieve satisfactory convergence at each cross section. After storing the most recently computed values as the upstream values, the calculations were advanced to the next downstream section. The end of the twisted-tape section was identified by a marker, and the solutions were completed in the annular section by suppressing all terms containing y in Table 1. At the inlet to the successive twisted-tape sections, axial recirculation was indeed encountered for the first two axial stations when $d/D \simeq 0.25$. When this situation occurred, negative axial velocities were put to 0 to avoid divergence. For $d/D < 0.25$, however, no axial circulation was encountered.

At each cross section, the local pressure gradient was evaluated to yield a local friction factor defined as

$$f_{\text{local}} = \frac{\partial \bar{P}^*}{\partial z^*} \tag{10}$$

Further, the pressure drop $\Delta\bar{P}^*$ over each module yielded the module-friction factor as

$$f_{\text{module}} = \frac{\Delta\bar{P}^*}{2(my+s)} \tag{11}$$

When the value of f_{module} over successive modules changed typically by less than 4 percent, the flow was declared as having reached the periodically fully developed state and the computations were stopped. Four percent was considered to be adequate, keeping in mind the accuracy of the experimental data. The computations indeed showed that the periodically fully developed state was always reached in 3 to 4 modules, irrespective of the values of y, s, and Re, as found by Saha *et al.*[6]

Heat transfer prediction

With the assumption of uniform fluid properties, the temperature equation was decoupled from the flow equations. The former equation was, however, solved using the velocity profiles of the periodically fully developed state. This departure from reality in the experiment was introduced by arguing that since the flow-mixing effects were sufficiently vigorous in both the inlet region as well as the periodically fully developed region, the use of the velocity profiles from the latter region will not have significant effect on the heat transfer predictions.†

The computations begin with the initial condition, Equation 8. For an axially uniform heat flux condition the bulk fluid temperature at each axial location is known *a priori* from the overall heat balance as

$$T_{b,\text{true}}^* = \frac{4\pi Z^*}{\text{RePr}} \tag{12}$$

The same, however, is not true of the wall temperature, which is determined as follows. At a downstream station guessing T_{wg}^* allowed the temperature equation to be solved. The computed temperatures permit the bulk temperature T_{bg}^* to be evaluated and checked against the true bulk temperature from Equation (12). The difference $\Delta T_b^* = T_{b,\text{true}}^* - T_{bg}^*$ is then added to all the fluid temperatures including that at the wall. Because of the linearity of the temperature equation, the temperatures thus corrected are the true solution, and no further refinement of the wall temperature is necessary.

† Although the situation considered is similar in some ways to the typical "thermal entry" problem, the solutions are not expected to be independent of the Prandtl number, as the velocity profiles do change at every cross section within a module.

The local Nusselt number now becomes

$$\mathrm{Nu}_z = \frac{hD}{K} = \frac{2}{\pi(T_w^* - T_b^*)} \tag{13}$$

The module-averaged Nusselt number is

$$\mathrm{Nu}_{\text{module}} \equiv \frac{1}{(my+s)} \int_0^{(my+s)} \mathrm{Nu}_z \, dz^* \tag{14}$$

and the length-averaged Nusselt number is

$$\overline{\mathrm{Nu}} = \frac{1}{N} \int_1^N \mathrm{Nu}_{\text{module}} dN \tag{15}$$

where N is the number of modules.

When the $\mathrm{Nu}_{\text{module}}$ changed by less than 1 percent between successive modules, the heat transfer was described as being thermally periodically fully developed. Typically between 20 and 50 modules were required to attain this fully developed state.

Computational details

All the computed results presented in the next section were obtained with 25 (radial) × 25 (circumferential) nodes that were nonuniformly spaced; closer spacings were provided near the walls. The number of nodes was arrived at after successive refinement of grid size, starting with a 15 × 15 grid. The friction factor (at Re = 1,250, $y = 3.3$, and $s = 2.5$) for a 25 × 25 grid differed from that for a 21 × 21 grid by less than 2 percent. Similar testing of the grid size for heat transfer predictions, however, was not carried out.

At the inlet to each section, the first axial step size was $\Delta Z^* = 2.5 \times 10^{-4}\,\mathrm{Re}$. Subsequently, however, the step size was often expanded by a maximum of 10 percent in the downstream direction, ensuring always that the prescribed length of the section was exactly covered.

3. Results

From the governing equations and boundary conditions—for the periodically fully developed state—the flow and the heat transfer characteristics are given by:

$$f_{\text{module}} = F\left(\mathrm{Re}, y, s, \frac{d}{D}, m, \frac{\delta}{D}\right) \tag{16}$$

and

$$\mathrm{Nu}_{\text{module}} = F\left(\mathrm{Re}, \mathrm{Pr}, y, s, \frac{d}{D}, m, \frac{\delta}{D}\right) \tag{17}$$

Computations were performed for the following parameter values:

$\mathrm{Re} = 500, 900, 1250$

$y = 5.0, 3.3$

$s = 2.5, 10$

$\frac{d}{D} = 0.25, 0.05$

$m = 1, 2, 3$

$\mathrm{Pr} = 5, 50$

$\frac{\delta}{D} = 0.0$

Recall that the experiments of Saha *et al.*[6] were conducted with $d/D \simeq 0.25$, $m = 1.0$, $\mathrm{Pr} \simeq 5.0$, and $\delta/D = 0.033$. In the computations, the last parameter was assumed to be zero to avoid the problem of having to consider nonorthogonal intersection of the grid lines with the tape boundary. The tape thickness δ, however, is known to have an effect (of the order of 7 to 10 percent) on the friction factor[5] in the case of full-length twisted tape. In the present configuration the tape thickness is unlikely to affect the module friction factor to the same extent, because the tape is interrupted by the rod connections. The neglect of the tape thickness thus appears justified.

Friction factor (compared to experiment)

Figure 3a and b shows the experimental data for four values of s and $y = 5.0$ and $y \simeq 3.3$. These values of y represent substantially tight twists of the tape. In the experiments, friction factors were evaluated from the pressure drop over the last three modules. For clarity, values of two times f_{module} are plotted.

Figure 3a and b also shows the present results ($m = 1$ and $d/D = 0.25$) for $s = 2.5$ and $s = 10.0$, as well as the correlation from[5] based on Date's computations[1] for the full-length twisted tape (i.e., $s = 0$). The predictions appear to be satisfactory at $y = 3.3$ (Figure 3b). They confirm the experimental finding that the friction factor for $s = 10$ is lower than that for $s = 0$ and that it is higher for $s = 2.5$. At $y = 5.0$ (Figure 3a), the friction factor

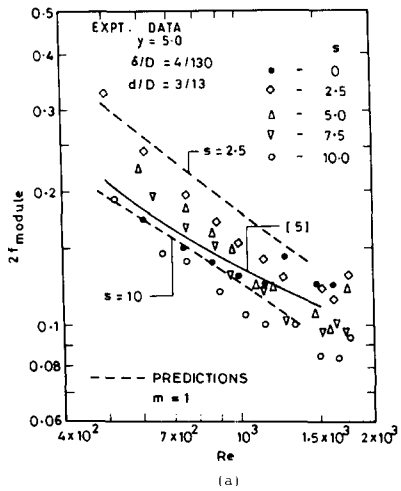

Figure 3(a) Effect of s on friction factor ($y = 5$)

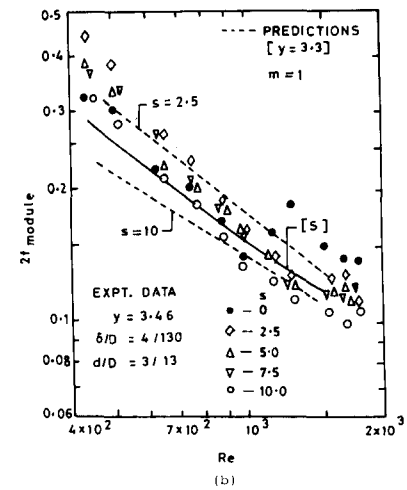

Figure 3(b) Effect of s on friction factor ($y = 3.46$)

Table 2 Predicted periodically fully developed friction factors (f_{module})

	$y=5.0$		$y=3.3$	
Re	$s=2.5$	$s=10$	$s=2.5$	$s=10$
500	0.146	0.0968	0.1565	0.1052
900	0.102	0.06617	0.09665	0.0752
1,250	0.0724	0.0513	0.0738	0.0545

is overpredicted (maximum of 15 percent) for both $s=2.5$ and $s=10$. The predicted friction factor for $s=10$, however, is still lower than that for $s=0$, as shown by the experiment. The estimated uncertainties associated with the experimental data are on the order of 6 percent, so the overall comparison appears to be satisfactory. Table 2 provides the exact computed values of f_{module}.

Nusselt number (compared to experiment)

Before presenting the comparison of the length-averaged Nusselt number $\overline{Nu}$, we need to point out the dissimilarities between the experimental and computational conditions. Recall that the experimental test section contained only 16 thermocouples for measuring wall temperature at different axial locations. Depending on the values of y and s, these locations could fall within either the tape section or the annular section of a typical module. From the experiments, the length-averaged Nusselt number was calculated from the local Nusselt number at 16 locations as

$$\overline{Nu}_{exper}=\frac{1}{Z}\int_0^Z Nu_Z\,dZ$$

If the local Nusselt number—as defined by Equation 13—were to vary significantly with Z within each module, this evaluation provides only an approximate length-averaged Nusselt number $\overline{Nu}$.

The predicted values of Nu_Z did indeed demonstrate significant axial variations (Figure 5), and the magnitudes of the length-averaged Nusselt numbers in the tape and the annular sections did differ in magnitude. A true comparison between the $\overline{Nu}$ of Equation 15 and $\overline{Nu}_{exper}$ defined in the preceding equation is possible only when several wall thermocouples are placed within a module length. Despite this difference, comparisons were made on the assumption that the Nu_Z in the experiment substantially represents the value of Nu_{module} (Equation 14).

Further, in the computations, the wall temperature at $Z=0$ was assumed to equal the bulk temperature. This meant that the predicted values of the Nu_{module} in the first two or three modules were very high compared to that in the experiment, where axial conduction in the wall effectively depressed the values of Nu in the inlet sections. This meant that $\overline{Nu}$ calculated according to Equation 15 was considerably higher than the $\overline{Nu}_{exper}$. To account for wall conduction, therefore, we ignored the computed values of Nu_{module} in the first two modules (or the lower limit of integration in Equation 15 was set at $N=3$).

Exact conditions at the inlet corresponding to those in the experiment could have been used in the computations. However, this approach would have meant performing computations only at the exact values (which were arbitrary) of the Reynolds numbers set in the experiments. This would have prevented any generalizations to be drawn from the computed results. Thus all computations were performed for fixed values of Re, and the results corrected as explained.

Finally, in carrying out the comparisons, care was taken to account for the following. In the experiment, the total number of modules was $167/(y+s)$ as mentioned previously. Thus at $y=5.0$ and $s=10$, for example, the test section provided for only 11 modules. The upper limit of integration in Equation 15 was thus chosen appropriate to the experimental conditions (i.e., $N=11$ in this case). In a way, this method accounted for the L/D effect on the length-averaged Nusselt number. Table 3 provides the exact computed values of $\overline{Nu}$ corresponding to the experimental conditions.

Table 3 Computed Nu values approximating the experimental conditions (Pr≃5.0)

	$y=5$		$y=3.3$	
Re	$s=2.5$	$s=10$	$s=2.5$	$s=10$
500	15.1 (22)†	13.4 (11)	19.02 (29)	14.10 (13)
900	27.0	23.5	33.2	23.15
1,250	33.8	30.0	44.5	30.5

† Numbers in parentheses show the relevant number of modules i.e. $167/(y+s)$.

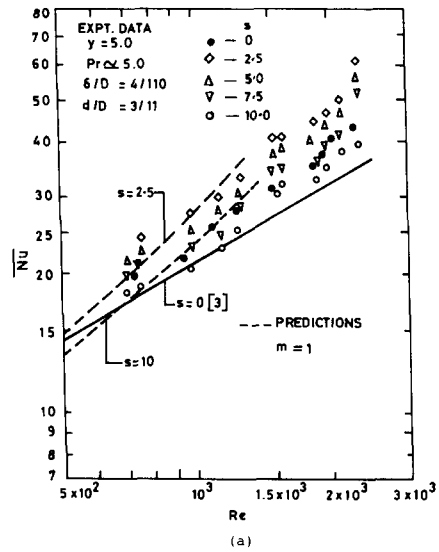

Figure 4(a) Effect of s on Nusselt number ($y=5$)

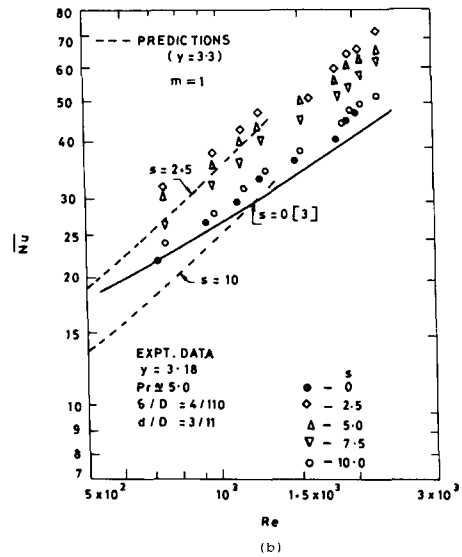

Figure 4(b) Effect of s on Nusselt number ($y=3.18$)

Figure 4a and b shows the comparison between $\overline{Nu}_{exper}$ and computed $\overline{Nu}$. At both values of y (=5 and 3.3), the predictions agree closely with the experiment for the spacing of $s=2.5$. At $s=10$ however, there is disagreement; at $y=3.3$ for example, underprediction of the order of 20 percent is noticed. Because the uncertainties associated with the experiment were estimated at nearly 10 percent, overall agreement appears to be satisfactory. Further, small discrepancies occur in the parametric values chosen for the computations. For example, in Figure 4b, a choice of $y=3.18$ and $d/D=3/11$—and allowance for tape thickness—would certainly push the predictions closer to the experimental data.

Further computed results

Variation of Nu_z within a module

Figure 5a and b shows a typical variation of Nu_Z in the thermally periodically fully developed region for $y=5$ and $s=10$ and $y=3.3$ and $s=2.5$, respectively, with $m=1$ and $d/D=0.25$ and $Re=900$ and $Pr=5.0$.

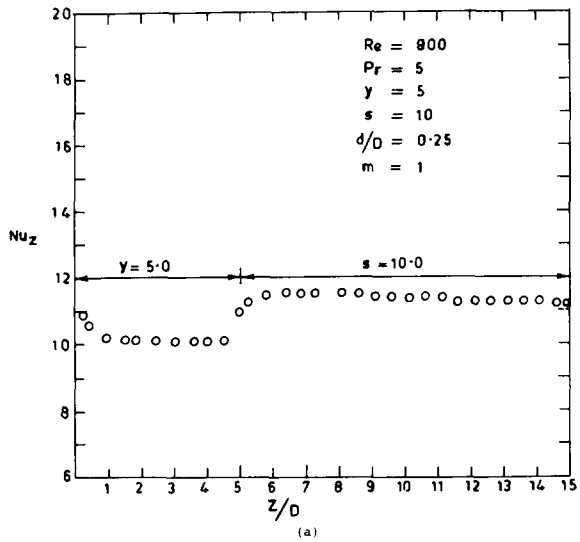

Figure 5(a) Variation of axially local Nusselt number along a module

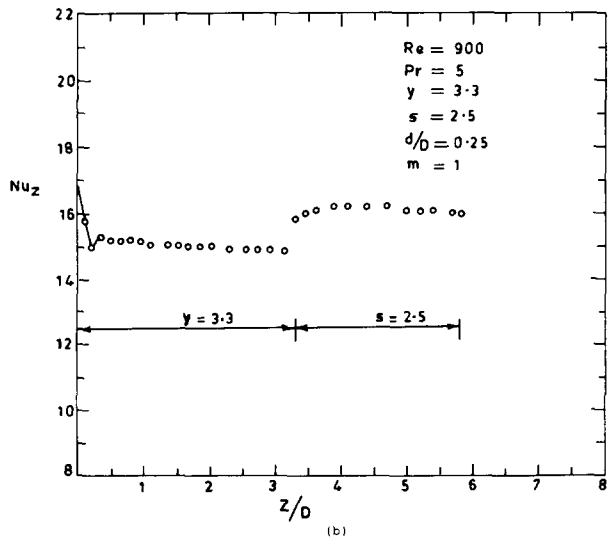

Figure 5(b) Variation of axially local Nusselt number along a module

Both parts of Figure 5 show that the Nusselt numbers in the annular section are higher than those in the twisted-tape section. Close examination of Figure 5a reveals further interesting features. The average value of Nu in the tape section is about 10.5, which is lower than the value of about 18 for full-length tape[3] at $Re=900$. However, the average value of Nu in the annular section is about 11.5, which is higher than the fully developed value of 6.56 for straight annular flow[10] with $d/D=0.25$. These values suggest that if a long tube were considered and the flow were allowed to attain the thermally periodic fully developed state, the Nusselt numbers with the present configuration would be lower than those with the full-length twisted tape of the same twist. Now if the comparisons in Figure 4 showed definite improvement with the regularly spaced, twisted-tape elements, it is only because of the strong L/D effect associated with this geometry. This observation further suggests that considerably improved performance can be expected from the present configuration at large Prandtl numbers.

Similar evaluation of the results presented in Figure 5b suggests that, with less space between tape elements, heat transfer deterioration may not be significant, even in long tubes.

Further, both parts of Figure 5 show a considerable reduction in Nu_z at the inlet to the tape section and a sudden rise in Nu_z at the inlet to the annular section. Because T_b^* increases linearly with Z^* at all axial locations, the peculiar variations in Nu_z are associated with the local values of $T_w^*(Z^*)$. At the inlet to the annular section, the fluid possesses substantial swirl and the fluid must "jump" the connecting rod. Also in the inlet region of the annulus, the flow tries to attain circumferential symmetry. These phenomena provide high velocities near the tube wall, thus suddenly reducing $T_w^*(Z)$ and hence a sudden increase in Nu_z. At the inlet to the tape section, the flow enters with a weak swirl and accelerates rapidly near the axis, where the swirl is further suppressed as the flow "jumps" from the rod. This action reduces the flow velocities near the tube wall, causing $T_w^*(Z^*)$ to rise and hence Nu_z to drop. Farther down the tape section, however, the swirl again increases and prevents the Nusselt number from falling any further.

Axial variation of Nu_{module}

Figure 6 shows the typical axial variation of Nu_{module} at $Re=900$ and $Pr=5.0$, demonstrating the strong effect of L/D on the Nusselt number. The number of modules required for attainment of thermally fully developed state were typically smaller for large y (small twist) and large s (large spacing) than those for small y and small s.

Table 4 Effect of Prandtl number ($m=1$ and $d/D=0.25$) on thermally periodic fully developed Nu_{module}

Re	$s=2.5$	$s=10$	$s=2.5$	$s=10$
		Pr=5		
500	8.6 (24)†	6.19 (20)	9.56 (26)	6.35 (22)
900	12.7 (26)	11.25 (20)	16.94 (26)	10.45 (22)
1,250	15.7 (29)	14.37 (21)	22.54 (27)	11.50 (24)
		Pr=50		
500	24.23 (43)	17.43 (34)	26.95 (47)	17.90 (36)
900	35.79 (45)	31.70 (32)	47.74 (47)	29.45 (37)
1,250	44.25 (48)	40.50 (32)	63.53 (48)	32.41 (41)

† Numbers in parentheses show the number of modules required to attain fully developed conditions.

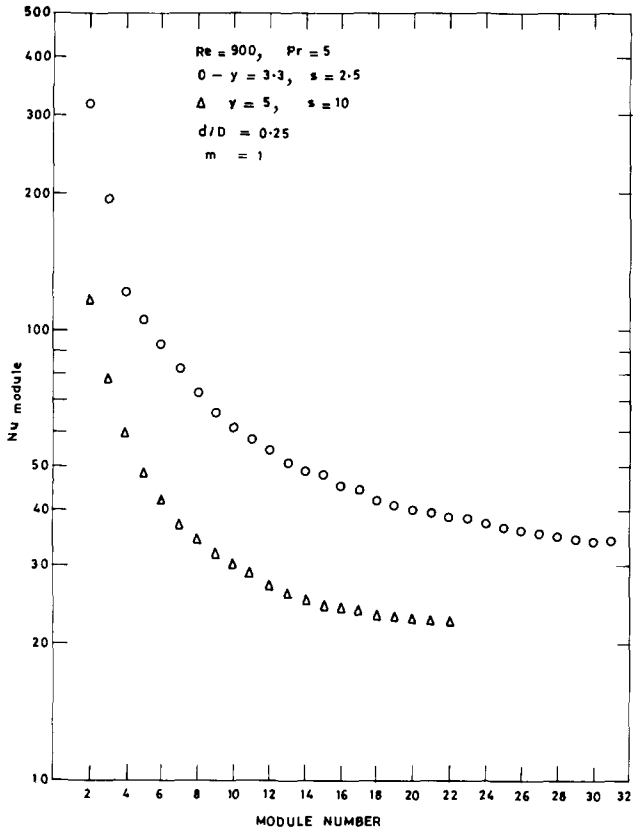

Figure 6 Axial variation of module-averaged Nusselt number

Effect of Prandtl number

Table 4 shows the predicted values of the thermally periodically fully developed Nu_{module} for $Pr=5.0$ and $Pr=50$. The predicted values at the higher Prandtl number, however, must be considered tentative. They were not checked with more refined mesh sizes, which would probably be necessary to resolve the thin thermal boundary layers. The Nusselt number is almost proportional to $Pr^{0.45}$. The exponent of the Prandtl number suggests turbulent flowlike characteristics under laminar flow conditions.

Effect of connecting rod diameter

Table 5 shows the computed values of the periodically fully developed f_{module} and Nu_{module} at two values of d/D, with $y=3.3$, $s=2.5$, $m=1.0$, and $Re=900$. For the small rod diameter case, the friction factor is 10 percent less and heat transfer increases significantly. The reason is that, when the local values of Nu_z within the module were examined as for those in Figure 5, the Nusselt numbers in the inlet region of the tape section no longer showed a sharp decline. In fact the Nu_z remained almost constant in both the tape and annular sections. Also, for the small-diameter case, negative axial velocities were not predicted even at the first axial step in the tape section, and thus the swirl was not suppressed. A small rod diameter thus has a favorable overall effect. Hence doing away with the connecting rod and locating the tape elements in place—probably by "pinching" the tube—may be desirable.

Effect of number of tape turns

Table 6 shows the computed values of fully developed f_{module} and Nu_{module} for three values of m at $y=3.3$: $s=2.5$, $Re=900$, and $d/D=0.25$. The f_{module} is marginally influenced by m. However the Nu_{module} for $m=3$ is nearly 25 percent smaller than that for $m=1$ at $Pr=5$, whereas at $Pr=50$ it marginally increases. As mentioned before, the results for $Pr=50$ must be considered tentative.

A more valid comparison, which would highlight the effect of m, however, should involve a fixed length of tube accommodating an exact number of modules. For $y=3.3$ and $s=2.5$, choosing $L/D=174$ would yield 30 modules for $m=1$, 19 for $m=2$, and 14 for $m=3$. Then the pressure-drop ratio ΔP_{ratio} over length L would be $19fm=2/30fm=1$ for $m=2$ and $14fm=3/30fm=1$ for $m=3$. These ratios are also shown in Table 6. They demonstrate a drastic reduction in pressure drop, which is in excess of the reduction in heat transfer. Thus it appears that on the basis of constant pumping power, the larger number of turns may yield improved thermohydraulic performance compared to the single turn on the twisted-tape element.

4. Conclusions

The following are the conclusions of the present paper:

(1) The friction factor and Nusselt number for laminar, developing flow in a tube containing regularly spaced twisted tape elements connected by thin circular rods were predicted by solving 3-D parabolic equations of momentum and energy transfer. Both flow and heat transfer reach a periodically fully developed state.

(2) The predicted friction factors agree well with the experimental data of Saha *et al.*,[6] whereas the Nusselt numbers agree well with the experimental data only for small spaces between the tape elements ($s=2.5$). For $s=10$, both under- and over-prediction by about 15 percent was observed.

(3) The effect of the Prandtl number on the Nusselt number is significant ($Nu \propto Pr^{0.45}$).

(4) The predictions show that considerably enhanced thermohydraulic performance can be achieved by reducing the connecting rod diameter and by providing more turns (instead of only one turn) on the twisted-tape elements.

Table 5 Effect of d/D on f_{module} and Nu_{module} at $y=3.3$, $s=2.5$, $Re=900$ and $m=1$

		Nu_{module}	
d/D	f_{module}	$Pr=5$	$Pr=50$
0.25	0.09665 (3)†	16.94 (26)	47.74 (47)
0.05	0.08685 (3)	21.75 (24)	97.8 (42)

† Numbers in parentheses represent the number of modules required to attain fully developed conditions.

Table 6 Effect of m on f_{module} and Nu_{module} at $y=3.3$, $s=2.5$, $Re=900$, and $d/D=0.25$

			Nu_{module}	
m	f_{module}	ΔP_{ratio}	$Pr=5$	$Pr=50$
1	0.09665 (3)†	1.0	16.94 (26)	47.74 (47)
2	0.1069 (3)	0.7	14.25 (25)	49.71 (47)
3	0.1104 (3)	0.533	13.15 (21)	51.97 (36)

† Numbers in parentheses represent the number of modules required to attain fully developed conditions.

Acknowledgments

This work was financially supported by the Council of Scientific and Industrial Research, Government of India, under the grant of CSIR 23 (158)/86 EMR-II.

References

1 Date, A. W. Prediction of fully developed flow in a tube containing a twisted tape. *Int. J. Heat and Mass Transfer*, 1974, **17**, 845–859

2 Date, A. W. Numerical prediction of laminar flow pressure drop and heat transfer in the entrance length of a tube containing a twisted tape. *Proc. 2nd Nat. Heat and Mass Transfer Conference* (Paper no. 3), I.I.T. Kanpur, India, 1973

3 Hong, S. W. and Bergles, A. E. Augmentation of laminar flow heat transfer in tubes by means of twisted-tape inserts. *Trans. ASME J. Heat Transfer*, 1976, **98**(2), 251–256

4 Sukhatme, S. P., Gaitonde, U. N., Shidore, C. S., and Kuncolienkar, R. S. Forced convection heat transfer to a viscous liquid in laminar flow in a tube fitted with a twisted tape. *Proc. 9th Nat. Heat and Mass Transfer Conference* (Paper no. HMT 7-87, Part B), 1–3, IISc., Bangalore, India, 1987

5 Shah, R. K. and London, A. L. Laminar flow forced convection in ducts. In *Advances in Heat Transfer*, Vol. 1, Suppl. 1, T. F. Irvine Jr. and J. P. Hartnett, eds. 1978, 379–381

6 Saha, S. K., Gaitonde, U. N., and Date, A. W. Heat transfer and pressure drop characteristics of laminar flow in a circular tube fitted with regularly spaced twisted-tape elements. *J. Exp. Thermal Fluid Sci.*, 1989, **2**, 310–322

7 Date, A. W. and Gaitonde, U. N. Development of correlations for predicting characteristics of laminar flow in a tube fitted with regularly spaced twisted-tape elements. *J. Exp. Thermal Fluid Sci.*, 1990, **3**, 373–382

8 Date, A. W. Prediction of friction and heat transfer characteristics of flow in a tube containing a twisted tape. Ph.D. Thesis, Imperial College, University of London, 1972

9 Caretto, L. S., Curr, R. M., and Spalding, D. B. Two numerical methods for three dimensional boundary layers. Dept. of Mech. Enr., Imperial College, London, Rep. No. HTS/71/16, 1971

10 Kays, W. M. and Crawford, M. E. *Convective Heat and Mass Transfer*, Tata McGraw-Hill, New Delhi, India, 1983